

Understanding the origin of Tabula Rasa-induced defects in n-type Cz c-Si: The case of nitrogen atmosphere

Jorge Ochoa ^a, Vincenzo LaSalvia ^b, Paul Stradins ^b, Mariana I. Bertoni ^{a,*}

^a School of Electrical, Computer and Energy Engineering, Arizona State University, 650 E. Tyler Mall, Tempe, 85287, AZ, USA

^b National Renewable Energy Laboratory, 16253 Denver West Parkway, Golden, 80401, CO, USA



ARTICLE INFO

Keywords:

Defects silicon
Bulk lifetime characterization DPCM
Surface passivation tabula rasa
Thermally induce degradation

ABSTRACT

Phosphorus-doped Czochralski-grown silicon (Cz-Si) has been gaining market share in the large-scale manufacturing of high-efficiency silicon (Si)-based photovoltaic (PV) devices thanks to higher carrier lifetimes than their boron-doped counterpart. However, the fabrication of n-type Cz-Si based solar cells often requires process steps with much higher temperatures and longer times than p-type Silicon. Defect interaction with the high temperatures during such processes tend to be detrimental to the n-type Cz-Si carrier lifetime, therefore limiting the final device efficiency. Short thermal anneals before cell processing, known as Tabula Rasa (TR), have been proposed to mitigate the thermally induced lifetime degradation during n-type Cz-Si solar cell fabrication. This work thoroughly investigates the defects responsible for the lifetime degradation after TR in a N₂ atmosphere treatment. We use temperature-injection-dependent lifetime spectroscopy and the thickness variation method to decouple the effects of TR treatment in the bulk and the surface of the n-type Cz-Si wafers. Using the defect parameter contour mapping (DPCM), we identify the defect energy level (E_t) and the capture cross-section ratio (k) of the most likely process-induced defect, which aligns with previously proposed Si vacancy-associated defects. The DPCM reveals that these vacancy-associated defects have a shallow energy level $E_t - E_v \sim 0.13$ eV and very efficient electron capture cross section $k \sim 600$. Unexpectedly, the bulk degradation due to vacancy defects in the volume of the wafer, is accompanied by a significant increase in the surface recombination as well. Through evaluating the surface recombination velocity temperature- and injection dependence, we show that after TR, at room temperature and for an injection level of 10^{15} cm^{-3} , in a wafer passivated with a-Si:H(i) the surface recombination dominates the overall lifetime response. We hypothesize that the near surface vacancy-associated bulk defects play a role in lowering the electron diffusion current into the a-Si:H(i) from the c-Si(n) reducing the field-effect passivation.

1. Introduction

Much has been reported about the defect resilience of n-type Silicon (Si) and its ability to reach much higher lifetimes than its p-type counterpart. Not only n-type wafers benefit from the absence of boron-oxygen related recombination centers, but are also considerably more resistant to recombination introduced by metal impurities and do not exhibit light-induced degradation (LID) [1–3].

Swanson and Smith [4,5] proposed a target bulk lifetime (τ_{bulk}) of 5 ms to obtain solar cell devices with efficiencies beyond 25% in production. n-type Czochralski silicon (Cz-Si) has emerged as an excellent candidate to achieve the minority carrier lifetimes conducive to these high efficiencies in production, and certain manufacturers have already

validated its potential [6,7]. However, grown-in oxygen defects in Cz-Si wafers that lead to ring defects [8] have been reported to impart n-type Cz-Si a certain sensitivity to high temperature processing steps, common during cell fabrication. These ring defects are caused by recombination active oxygen precipitates and their associated extended defects [9] which strongly degrade the minority carrier lifetime reducing the device performance [10,11]. This thermally induced degradation (TID) of the minority carrier lifetime is considerably stronger in upgraded metallurgical-grade (UMG) than in electronic grade (EG) n-type Cz-Si since the first contains a higher concentration of both metallic and nonmetallic impurities, in addition to the grow-in oxygen precipitates [12].

Drawing an analogy to the integrated circuit (IC) industry, which has

* Corresponding author.

E-mail address: bertoni@asu.edu (M.I. Bertoni).

accelerated the development of processes and strategies to maximize performance for the case of n-type Si, a modified short thermal anneal preceding cell processing, known as Tabula Rasa (TR), has been proposed for the photovoltaic (PV) industry as a promising approach to mitigate the TID of the carrier lifetime [10–12]. The IC industry employs rapid thermal annealing (RTA) as a method to control and engineer intrinsic point defects with the goal of changing and regulating oxygen-related defects in Si [13]. The lifetime resilience after RTA has been attributed to the behavior of oxygen precipitates and especially to the dissolution of built-in oxygen precipitate nuclei [13,14].

LaSalvia et al. [11] showed that TR is an effective method for dissolving oxygen precipitate nuclei in PV n-type Cz-Si and makes this material resistant to TID. The authors report that regardless of the gas environment (inert or oxidizing), remarkably, TR makes n-type Cz-Si wafers significantly more resistant against TID after high temperature processing such as the standard thermal budget for Boron diffusion. Intrinsic point defects, created during Cz growth and introduced or mitigated by the thermal process, govern the degradation and resilience of the carrier lifetime in n-type Cz-Si [11]. In the case of TR performed in an inert atmosphere (N_2), the minority carrier lifetime is reduced dramatically immediately after the RTA process [11]. The carrier lifetime degradation after TR in N_2 is such that the process appears unsuccessful or even detrimental to cell performance. However, the wafer carrier lifetime recovers to values compatible with high-efficiency device manufacturing after a second thermal budget mimicking the B-emitter formation. LaSalvia suggests that vacancies resulting from TR treatments in N_2 are responsible for the lifetime degradation after the TR process. These vacancy defects anneal out during the second thermal budget, explaining the resilience of the carrier lifetime [11]. However, the authors did not identify defects conclusively nor separate the contributions to the bulk and surface recombination. A similar study performed in p-type Cz-Si by Meyer et al. [15] supports the theory of the lifetime degradation due to Si vacancies, but again, without a detailed carrier lifetime spectroscopy analysis.

In this contribution, we study the effect that TR ($1100\text{ }^\circ\text{C}$ for 10 min) processing in an inert ambient (N_2) has on n-type Cz-Si by thoroughly characterizing the surface recombination velocity (SRV) and τ_{bulk} [16] as a function of injection and temperature before and after treatment. We choose to study TR in N_2 as the previous work by LaSalvia et al. [11] in n-type c-Si and by Meyer et al. [15] in p-type c-Si report that other TR ambient process conditions does not induce carrier lifetime degradation. We use temperature-injection-dependent lifetime spectroscopy (T-IDLS) and the defect parameter contour mapping (DPCM) to visualize the combinations of defect energy level (E_d) and capture cross section ratio (k) that best fit the TR-induced behavior [17]. We show that the E_d and k combinations for the most likely bulk lifetime limiting defects, immediately after TR in N_2 seem to be related to vacancy-associated defects in line with the results reported by LaSalvia et al. [11]. By evaluating the SRV temperature- and injection dependence, our results also suggest that the defects induced by TR have a dominant effect on the SRV at room temperature.

2. Experiment

Figure 1 depicts the general process flow followed in this work. n-type Cz-Si wafers with a bulk resistivity of $2.5\text{ }\Omega\text{cm}$ from an ingot with a range $1\text{--}5\text{ }\Omega\text{cm}$, crystal orientation (100) , oxygen concentration $>15\text{ ppm}$, and an initial thickness of $190\text{ }\mu\text{m}$ were used for this study. Note that the bulk resistivity was measured before and after the TR treatment and we did not observe any changes. The wafers were subjected to a pre-cleaning in Piranha and RCA-2 solutions. Sets of different thicknesses were obtained by etching for different times with an acidic mixture of hydrofluoric, nitric, and acetic (HNA) at a rate of approximately $10\text{ }\mu\text{m}/\text{min}$. Four different thicknesses were achieved in the range of $105\text{--}175\text{ }\mu\text{m}$. The substrates were then subjected to a complete cleaning using RCA-2, Piranha, and a final dip in diluted hydrofluoric acid solution,

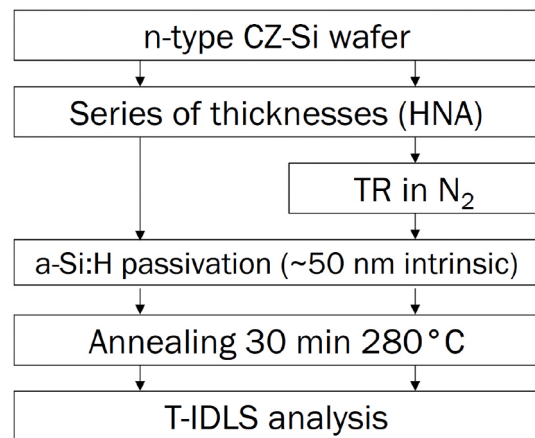


Fig. 1. Experimental process flow.

sequentially. One set received a TR-treatment in a conventional hot-wall tube furnace with pure N_2 gas ambient, at the National Renewable Energy Laboratory. The TR anneals were performed in a conventional hot-wall tube furnace at $1100\text{ }^\circ\text{C}$ for 10 min. The tube furnace has a N_2 gas ambient with a constant flow set at approx. 3.0 L/min . The furnace is a Tempress model 203-6, and the loading and unloading of the wafers into and from the hot zone are done manually with a quartz push rod. The exact protocol for TR-treatment can be found in Ref. [11]. Another set was held back from any TR treatment for evaluation of the as-received lifetime and used as a baseline. After the TR treatment, surface cleaning consisted of native oxide stripping in a dilute HF solution, and a sequence of wet chemical treatments for 10 min followed by a 10-min rinse in DI water. The wet chemical processing included the use of RCA-2 followed by Piranha and a final bath in BOE solution to ensure the removal of the silicon dioxide layer before the passivation layer deposition. The clean wafers were immediately passivated by depositing 50 nm of a-Si:H(i) on both sides using plasma-enhanced chemical vapor deposition (PECVD) technique in an Octopus I tool from INDEOtec SA following our methodology to fabricate symmetrically passivated structures [16]. The a-Si:H(i) layers were deposited at $220\text{ }^\circ\text{C}$ with a Silane to Hydrogen ($SiH_4:H_2$) gas ratio 40:200 in reactors powered at 13.55 MHz.

Effective minority carrier lifetime measurements at temperatures between 30 and $210\text{ }^\circ\text{C}$ were performed with the WCT-120TS tool from Sinton Instruments, where the effective lifetime was measured as the temperature decreased in transient mode since the measured effective lifetimes are greater than $200\text{ }\mu\text{s}$. As mentioned above, the main goal of this study is a detailed spectroscopy analysis of the carrier lifetime degradation, therefore the analysis focuses on the low-level injection regime, where SRH is dominant. The data was then processed using a 2-point slope with Savitzky-Golay filter derivative calculation routine for the lifetime determination. This derivative method provides a cleaner signal with lower noise levels for the analysis of lifetimes at low carrier densities. A detailed discussion covering the derivative methodology is included in Appendix A. As widely described by S. Rein and co-authors [18,19] as well as J. Schmidt [1], Injection Dependence Lifetime Spectroscopy (IDLS) by itself is ambiguous for the parametrization of Shockley Read Hall (SRH) defects. The defect parameters are confined to a solution surface where an infinite number of solutions of the defect parameters exists. Thus, by studying the lifetime as function of temperature, T-IDLS could potentially identify the correct solution [20]. In addition, because we are measuring thin wafers, $175\text{ }\mu\text{m}$ or less, the WCT-120TS has been calibrated to account for the coil sensitivity, see Appendix A for details. It is worth mentioning that as described by Black and Macdonald [21], the calibration is needed because the thickness of the wafers used for calibration ($525\text{ }\mu\text{m}$) is so different to those measured here ($175\text{ }\mu\text{m}$). Such difference can result in an overestimation

of the conductance, inducing errors in the measured lifetime that are significant for applications when the analysis is interested in lifetime behavior in high-injection because the lifetime in this regime is strongly dependent on the carrier concentration [21]. However, for defect characterization and SRH fitting, the mid-injection regime contains more valuable spectroscopic information than that at higher injections, where Auger recombination dominates. Regardless, we carried out the calibration for clarity on the measurement accuracy. For additional details about the fabrication of the symmetrical structures and lifetime measurements see Ref. [16]. The properties of the a-Si:H(i)/c-Si(n) interface were probed by decoupling the effects of the RTA treatment in the bulk and the surface from the measured effective lifetime using the thickness variation method. This allows to determine the SRV for every injection level at every measured temperature.

3. Results

It is well known that for symmetrically passivated samples with a minority carrier diffusion length greater than the sample thickness (W) and low SRV, the effective lifetime (τ_{eff}) can be expressed as [22]:

$$\frac{1}{\tau_{eff}(\Delta n, T)} = \frac{1}{\tau_{bulk}(\Delta n, T)} + \frac{2SRV(\Delta n, T)}{W} \quad (1)$$

$$\frac{1}{\tau_{bulk}} = \frac{1}{\tau_{SRH}} + \frac{1}{\tau_{Auger}} + \frac{1}{\tau_{rad}} = \frac{1}{\tau_{SRH}} + \frac{1}{\tau_{int}} \quad (2)$$

Where the τ_{bulk} can be subsequently expressed as the harmonic sum of the Shockley Read Hall (SRH) and intrinsic recombination components (τ_{int}) (Eq. (2)). Equation (1) allows to separate the contribution of bulk and interface to τ_{eff} by measuring τ_{eff} on a set of samples with different substrate thickness, W . The main assumption is that the τ_{bulk} (Eq. (2)) remains unchanged for a given injection level and temperature. When the inverse of the effective lifetime is plotted against the inverse of the sample thickness ($1/\tau_{eff}$ vs. $1/W$, Appendix Fig. 16) a linear relationship is revealed, where the slope of the line is equal to two times the SRV (Eq. (1)). This process is repeated for every injection level (Δn) and for each temperature (T) to obtain $SRV = f(\Delta n, T)$. The details of this methodology can be found in Refs. [1,16,18]. It is worth mentioning that the T -dependence of the parameters used to model the τ_{int} , namely Auger and radiative recombination mechanisms, have been experimentally determined by others [23,24] for a window of injections and temperatures narrower than the one considered here. In the case of the radiative recombination, temperature models exist, and they are widely accepted [25]. However, it is well known than in the case of Silicon, the Auger recombination dominates the intrinsic limit and no accepted

temperature parametrization exists. Studies by Bernardini et al. [16] showed that interestingly, the determined bulk lifetime is found to perfectly match the Auger limit at 150 °C while any curve at higher temperature surpasses the Auger limit. We believe that this originates from two issues, (1) as mentioned above, the lack of a proper Auger parametrization at higher temperatures, (2) possible inaccuracies of the mobility models being used in the Sinton lifetime tester. For the sake of accuracy and reporting values with small error we limit the SRH analysis to temperatures below 150 °C. In contrast, the study of the surface recombination is independent of the τ_{int} . Hence, we evaluated the SRV response in the range of temperatures 30–210 °C.

Figure 2(a) shows the τ_{eff} for the baseline wafer. For simplicity, we only present the thickest sample of the set ($W = 175 \mu m$), which exhibits a τ_{eff} above 3.5 ms. After an initial increment in the temperature range from 25 °C to 60 °C, the τ_{eff} decreases monotonically with increasing temperature. This trend tends to disappear with increasing injection level as the τ_{eff} starts to be limited mainly by the Auger recombination mechanism. This same τ_{eff} temperature behavior has been observed by other authors [16,26] and it has been linked to the T -dependence of recombination mechanisms happening at the c-Si surface rather than in the c-Si bulk. This is validated by the temperature dependence of the surface observed in Fig. 2(b), which shows that high temperature values for the measured τ_{eff} , are strongly dominated by the surface recombination. The SRV T -dependence corresponds to the reduction of the τ_{eff} from Fig. 2(a); therefore, the surface recombination is expected to dominate at high temperatures in agreement with the results reported in Ref. [16]. It is worth mentioning that the resulting SRV values (shown in Fig. 2(b)) in the temperature range investigated here are <2 cm/s, which are in line with previous reports for this passivation layer and allows the straight forward determination of the τ_{bulk} [16,17,26]. The calculated τ_{bulk} can be seen in Fig. 2(c), which contrary to Fig. 2(a) shows the expected temperature behavior for the bulk of a semiconductor [16,27]. Results for TR treated samples are presented in Fig. 3, showing the significantly degraded τ_{eff} (<300 μs) in agreement with observations by LaSalvia et al. [11]. For the sake of clarity on the accuracy of the measured lifetime we consider worth to mention that the maximum available carrier density (maximum minority carrier density of the measurement) is given by the lifetime-generation product (τG). Regardless of the photoconductance measurement methodology, QSS or transient, for reaching higher carrier density, higher illumination intensity must be used. To increase the maximum available carrier data, one can lower the flash closer to the sample in the WCT-120TS setup, however the reference cell can saturate causing inaccurate data to be reported. We optimized the height of the light to our measured lifetimes, see Appendix A for more details. The data points shown in the greyed

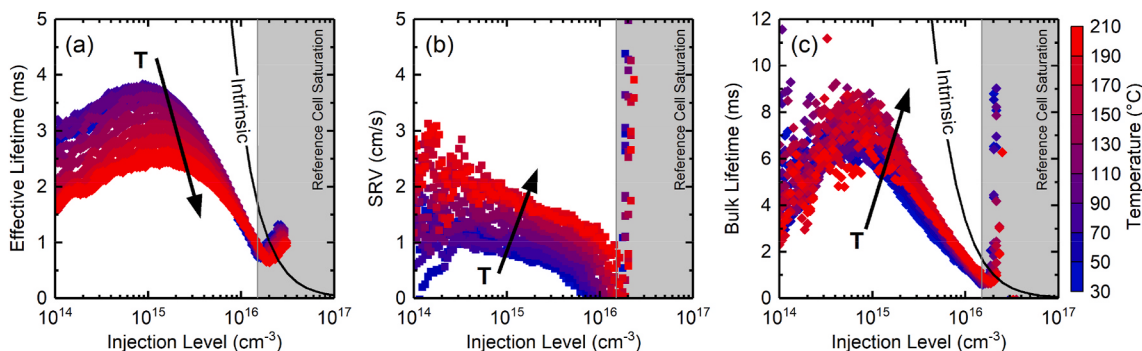


Fig. 2. (a) τ_{eff} for the thickest sample ($W = 175 \mu m$) as a function of injection level at temperatures with $10^\circ C$ step size for a n-type Cz-Si baseline sample (no TR processing) passivated with a-Si:H(i). The effective lifetime is calculated using 2-point slope with Savitzky-Golay derivative method. The Savitzky-Golay filter improves the signal noise which enhance the accuracy without distorting the signal tendency at low injection levels. See Appendix A for details. (b) Experimentally evaluated SRV for the a-Si:H(i) passivation layer as a function of injection level at temperatures with $10^\circ C$ step size. (c) Determined τ_{bulk} as a function of injection level at temperatures with $10^\circ C$ step size. The data inside the greyed, $\Delta n > 1.5 \times 10^{16} \text{ cm}^{-3}$ is inaccurate because of the saturation of the reference cell and so it is discarded.

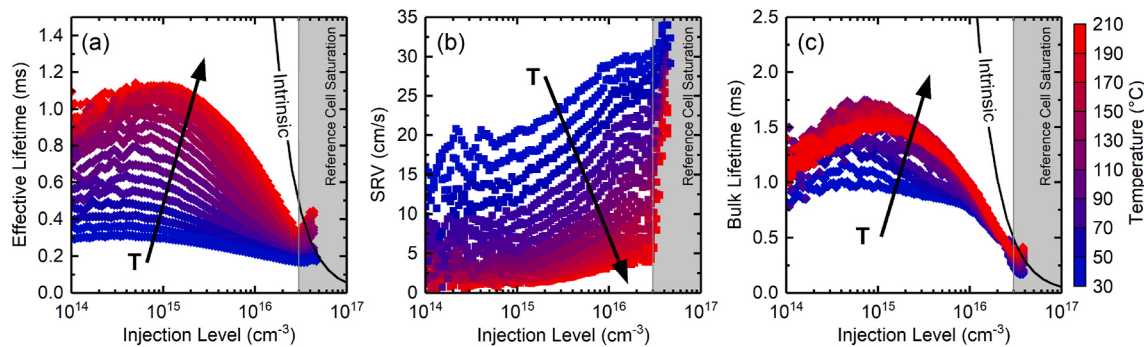


Fig. 3. (a) τ_{eff} for the thickest sample ($W = 175 \mu\text{m}$) as a function of injection level at temperatures with 10°C step size for a n-type Cz-Si sample treated for TR in N_2 and passivated with a-Si:H(i). TR in N_2 significantly degrades the effective lifetime. The effective lifetime is calculated using 2-point slope with Savitzky-Golay derivative method. The Savitzky-Golay filter improves the signal noise which enhance the accuracy without distorting the signal tendency at low injection levels. See Appendix A for details. (b) Experimental evaluated SRV at temperatures with 10°C step size. The obtained SRV suggests that TR in N_2 impacts the surface of the n-type Cz-Si. (c) Determined τ_{bulk} as a function of injection level at temperatures with 10°C step size. The data inside the greyed, $\Delta n > 3 \times 10^{16} \text{ cm}^{-3}$ is inaccurate because of the saturation of the reference cell and so it is discarded.

areas of Figs. 2 and 3, high level injection, is consequence of the saturation of the reference cell (G), which make these data points invalid for the lifetime spectroscopy analysis, hence they are discarded. Note that the goal of this study is to evaluate the lifetime data in the injection level raging from $5 \times 10^{14} \text{ cm}^{-3}$ to 10^{16} cm^{-3} as this is the range of injections that exhibits the most valuable spectroscopy lifetime data for a SRH analysis. We show the discarded data in Figs. 2 and 3 for transparency on the measurement accuracy.

A comparison of T-dependence for the baseline τ_{eff} and the TR in N_2 τ_{eff} reveals that the latter exhibits a completely reversed temperature dependent behavior. This would suggest that the intrinsic bulk response and the temperature dependence of the SRH recombination mechanisms dominate the τ_{eff} after TR in N_2 . The main contribution to such temperature behavior, however, appears to come from the SRV. The assessment of the SRV after TR in N_2 (shown in Fig. 3(b)) reveals that the TR treated wafers SRV is surprisingly much higher than the SRV observed in the untreated wafers (about 17 times, from 1 cm/s to 17 cm/s) and that the former one exhibits a much stronger temperature dependent response. The experimental evaluated injection and temperature-dependence SRV is evidence that the T-dependence of the SRV dominates the measured τ_{eff} after TR in N_2 . This assessment confirms that the assumption $\tau_{\text{bulk}} = \tau_{\text{eff}}$ does not hold for this study [22], and as such any inference on the type of defects or mechanisms at play is incorrect. Our analysis suggests that TR in N_2 could also impact the surface of the c-Si. With the known SRV, the actual injection and temperature-dependence of the bulk is revealed form Eq. (1) for accurate characterization of the most likely defect limiting the τ_{bulk} (shown in Fig. 3(c)). TR in N_2 treatment has degraded the τ_{bulk} about 4 times from 4 ms to 1 ms , but not as much as the measured τ_{eff} would directly suggest. In the following sections we examine the reduction by TR in N_2 of the τ_{bulk} and the increase of the SRV separately.

4. Discussion

4.1. τ_{bulk} limiting defects after TR treatment in N_2

Many authors have reviewed the effects of RTA on the intrinsic defect population and in particular the formation of vacancies [28,29]. It is known that by varying the soak temperature, soak times, cooling rates, and ambient conditions, it is possible to achieve a wide variety of vacancy concentration profiles in thin silicon wafers [30]. These conditions and the resulting vacancy concentration profiles have been studied extensively by several authors [30,31]. The current understanding suggests that at TR temperatures of 1100°C , the Si-Si covalent bond breaks forming Frenkel pairs, creating vacancies and interstitials in

the Si host material at equal rates. However, as noted by Voronkov and Falster those two intrinsic point defects have different diffusion coefficients [32]. Unlike electrons and holes, which always recombine in pairs, Frenkel pair defects can be annihilated in two ways: (1) recombine in the bulk by reoccupying the empty Si lattice sites left behind or (2) annihilate at the surface, by adding or subtracting Si surface atoms. By removing the Si wafer quickly-enough from the furnace, and effectively lowering the temperature so that no more Frenkel pairs are generated, an imbalance of intrinsic defects is generated. This imbalance originates from the fact that the interstitials (of the Frenkel pair) have a faster diffusion coefficient $\sim 10^{-3} \text{ cm}^2/\text{s}$ than the vacancies $\sim 10^{-4} \text{ cm}^2/\text{s}$ at 1100°C . Interstitials reach the surface faster, leaving behind a surplus of vacancies short of the sample surface.

Much of our knowledge of the structure and electronic properties of vacancies in Si is based on EPR and DLTS investigations by Watkins, Troxell and Newton [33–36]. These reports [34,35] established that the energy level above the valence band, at $E_t - E_v = 0.13 \text{ eV}$ corresponds to the second ionization energy of the silicon vacancy double donor, $V_{\text{Si}}^{**}(+/2+)$, while the first ionization energy, $V_{\text{Si}}^*(0/+)$, sits even closer to the valence band at $E_t - E_v = 0.05 \text{ eV}$, as a result of a large Jahn-Teller relaxation in the neutral charge state (see Fig. 4). Newton [34] showed by means of DLTS that the considered $E_t - E_v = 0.13 \text{ eV}$ defect level has

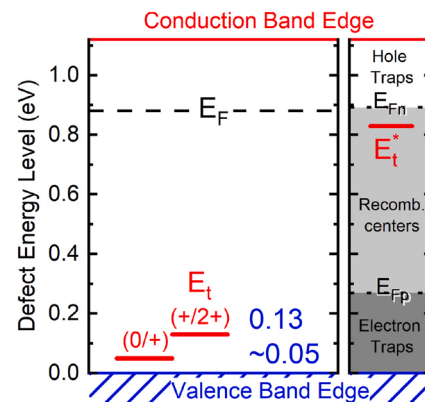


Fig. 4. Donor level positions for the vacancy defect. Greater Jahn-Teller relaxation for the neutral charge state causes a level inversion with the first donor state $(0/+)$ below the second $(+/2+)$. E_F shows the Fermi level for the n-type wafers used in this study. E_{Fn} and E_{Fp} divide the forbidden energy gap into three regions. Based on Stockmann methodology [33], a defect is classified according to the region into which its classification level E_t falls. Using the defect parameters obtained via the DPCM in this study, the vacancies defects are classified as a recombination center at room temperature.

no long-range Coulombic attraction for a hole according to the Poole-Frenkel theory confirming the donor-like characteristics of the defect level.

LaSalvia et al. [11] reported a donor vacancy with a shallow energy level $E_t - E_v = 0.11$ eV as the most likely lifetime-limiting defect after such RTA treatment. This energy level for the vacancy defect was determined using temperature-dependent lifetime spectroscopy (TDLS) [18] at a low injection level of approximately 10^{14} cm^{-3} . The TDLS analysis is limited to one injection level, and the authors assume a direct correlation of the bulk lifetime with the effective lifetime, $\tau_{\text{bulk}} = \tau_{\text{eff}}$, which as mentioned before is incorrect. To validate the presence of vacancy-associated defects as the most likely bulk lifetime-limiting defect after TR treatment in N₂, we follow the DPCM methodology [17], where the goodness of fit of the SRH model, for a broad combination of E_t and k values, is evaluated versus the extracted τ_{bulk} across a temperature range from 30 to 150 °C and an injection level from $5 \times 10^{14} \text{ cm}^{-3}$ to 10^{16} cm^{-3} . The DPCM evaluates the quality of the fit obtained for each combination of E_t and k values through the calculation of the average residual value (ARV) (see Bernardini et al. [17] for more details). The result is visualized on a single comprehensive plot. This plot is characterized by a color scale representing the ARV to readily identify the parameter space giving the best fits of the experimental data. Note that a main assumption here is that the lifetime is dominated by only one defect level – for details and discussion of multiple defect levels, see Refs. [16,38] respectively. Figure 5 shows the contour plot, where some characteristic bright areas corresponding to an ARV < 20% reveal the best-fit combinations of E_t and k for this defect. As expected, the (E_t , k) values resulting in a good fit are symmetric for k -values close to unity because defects with the same energy level distance from either the valence or the conduction band have virtually the same recombination strength [1]. Shallow defects with $E_c - E_t$ or $E_t - E_v < 0.2$ eV and symmetric k -values are suitable for describing the injection-dependent bulk lifetime curves.

A characteristic bright area, shown in Fig. 5 by the black line dashed contour, appears in the contour plot corresponding to an ARV below 10% which can be considered as an acceptable fit taking into account the errors associated with the methodology [39] and uncertainties in models employed [24]. Deep donor vacancy-associated defects separated from the valence band by $E_t - E_v = 0.13$ eV reported in the literature [33] denoted with a dashed white line fall into this characteristic bright area, where the lowest ARV can be obtained at the intersection of the dash line and a capture cross section ratio $k \sim 600$ (star on Fig. 5). Since the characteristic capture cross-section of electrons (σ_n) and the capture

cross-section of holes (σ_p) of a defect and thus the corresponding capture time constants may differ by orders of magnitude, it should be mentioned that the symmetry factor k parameter represents the characteristic extent of the capture asymmetry of the defect state, $k = \sigma_n/\sigma_p$. In addition to the assessment of the defect parameters, the time constant of holes (τ_{p0}) associated with the best fit to the τ_{bulk} shape at room temperature is estimated during the DPCM analysis [17]. The knowledge of the τ_{p0} allows the calculation of the defect density (N_t) from $\tau_{p0} = (N_t \sigma_p v_{th})^{-1}$, assuming a hole capture cross-section (σ_p) 10^{-16} cm^2 for vacancies [33] and using the thermal velocity $v_{th} = 2.1 \times 10^7 \text{ cm/s}$. A defect density $N_t = 6.9 \times 10^{11} \text{ cm}^{-3}$ is obtained, which is in line with the estimated densities from previously reported profiles of installed vacancies in Si [29,30].

While the energy level of donor vacancies seems to be established (Fig. 4), to the best knowledge of the authors, the capture cross section ratio parameter k has not been reported before. To understand the high efficiency for capturing electrons, $k \sim 600$, determined in this study, it is first important to mention that the SRH statistics assume that the semiconductor is in non-equilibrium conditions, i.e. hole-electron pairs are being generated at a constant rate by light or by some form of carrier injection, and the occupation probabilities and SRH recombination rates are calculated for steady-state conditions, which means the net rate of capture of electrons must be equal to that of holes [27]. The strong n-type characteristics of the wafers used in this study play an important role in the occupation probability and in the statistics of the so-called SRH densities for electrons and holes n_1 and p_1 . The vacancy-associated defect energy level is so close to the valence band that $E_F > E_t$, this corresponds to a high density of SRH holes at the defect level $p_1 \gg n_1$ and sufficient electrons $n_0 \gg n_1$ that an electron recombines at once with every hole [27]. Having f_t as the probability of occupation of a defect level by an electron and $f_{tp} = 1 - f_t$ as the probability of a defect level being empty, under illumination the defect capture electrons and holes at the rates $\sigma_n n_1 f_t = \sigma_p p_1 f_{tp}$, the excess SRH hole density p_1 is compensated by a higher efficiency for electron capture σ_n [27,37], therefore k is expected to be greater than 1. Based on Stockmann methodology [37], a defect is classified according to the region into which its classification level E_t^* falls in the forbidden energy gap. Figure 4 shows that the classification level E_t^* , as a result of the capture asymmetry of the defect state $k = \sigma_n/\sigma_p = 600$, falls between both quasi-Fermi energies E_{Fn} and E_{Fp} of the electrons and holes, thus the defect can be classified as a recombination center.

A donor-like level is positively charged when ionized, and neutral when occupied by an electron. With the vacancy-associated defect being close to the valence band, it cannot thermally emit electrons (the energy

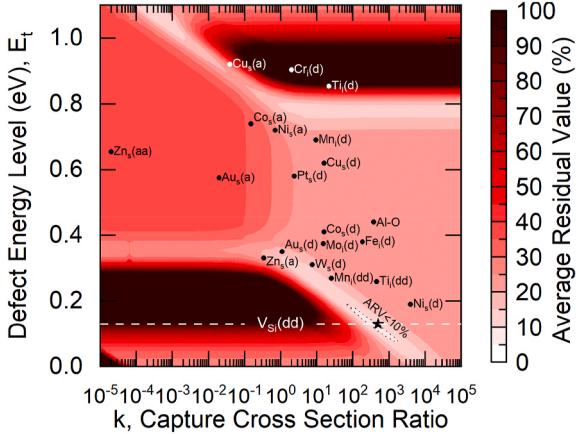


Fig. 5. Contour plot showing the quality of fit for τ_{bulk} averaged over different temperatures across a range from 30 to 150 °C. Bright areas reveal a good fit to the SRH model. The dashed line in relation to the reported energy level of V_{Si} [30] defect is indicating that the k -value has not been reported yet. The lowest ARV can be obtained at the intersection of the dash line and a k of 600 (star).

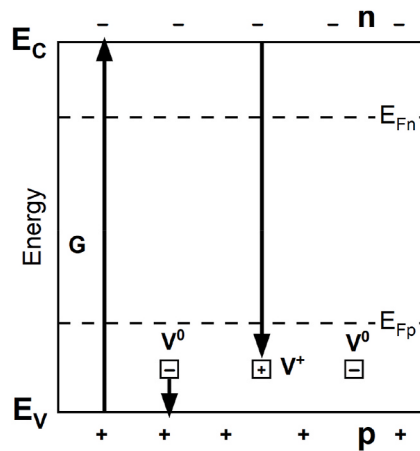


Fig. 6. Possible Interaction mechanism of free electrons with the vacancy-defect level for non-equilibrium conditions. The defect level cannot thermally emit electrons. Capture electrons need to wait for a photo-generated hole to get recombined with it.

distance is too large, Fig. 6), but it can thermally emit holes at a high rate. As the temperature increases any captured hole will get almost immediately emitted, returning the donor to a neutral state, while any captured electron will need to wait for a photo-generated hole to get recombined with it. This leads to a probability of occupation of the defect level with electrons f_t , being very close to 1, hence the lifetime is expected to increase. Unexpectedly, this is not the case for temperatures above 150 °C (Fig. 3(c)). It should be emphasized however, that as mentioned previously, the characterization of the defect parameters employing the DPCM methodology is restricted to temperatures below 150 °C and assumes that the lifetime is dominated by only one defect level. A closer inspection to the baseline τ_{bulk} (Fig. 2(c)) reveals that prior any TR treatment, the Si material displays a similar τ_{bulk} temperature dependence beyond 150 °C. This suggest that the τ_{bulk} exhibits what we presume is the signature of a second defect. Naerland et al. [38] demonstrates that the identification of two simultaneously occurring defects is highly ambitious and sometimes not practically feasible, thus we do not include the lifetime spectra for temperatures above 150 °C in our analysis. Furthermore, lifetime spectra at temperatures above 150 °C do not add relevant spectroscopy information and more important, the spectra is not operationally relevant, such temperatures are far from the operation conditions of solar cells.

4.2. TR in N_2 and the degradation of the SRV

The silicon lattice terminates abruptly at the surface, introducing a significant density of states within the bandgap. Because of the large density of surface states, the Fermi level becomes pinned at these surface states energy level in many semiconductors [40]. These bandgap states act as recombination centers leading to a significant surface recombination rate. Surface passivation mitigates this harmful recombination by combining two fundamentally different approaches: chemical passivation and field-effect passivation [41]. The chemical passivation reduces the surface state density to lower the carrier recombination probability, while in the field-effect passivation (as electrons and holes always recombine in pairs) the recombination is reduced when the surface density of one carrier type is diminished. In this work, we make use of the excellent passivation provided by intrinsic amorphous Silicon (a-Si:H(i)). The high-level of passivation is attributed to a very low defect density at the a-Si:H(i)/c-Si(n) interface, assisted by the incorporation of hydrogen into the films, which migrates to the interface and passivates the c-Si dangling bonds reducing the density of recombination centers [42,43]. Since c-Si surface defects are identified predominantly as dangling bonds, Olibet et al. [44] proposed to model the heterostructure interface recombination a-Si:H/c-Si by amphoteric defects, i.e. dangling bonds possessing three possible charge states, in contrast, the standard SRH recombination model is based on interface defects having an energy level within the band gap and two possible charge states. Details for the amphoteric model on dangling bonds can be found in Ref. [44]. The amphoteric model also explains the influence of the c-Si doping type and level on the surface passivation mechanism of a-Si:H(i). In addition to reducing the density of recombination centers, the passivation of strongly n-type doped Si wafer with a-Si:H(i) results in the diffusion of electrons into the a-Si:H where they occupy dangling bonds bandgap states. Therefore, the average charge density at the interface becomes more negative, leaving a positively charged space-charge region at the c-Si surface (see band diagram Fig. 7(a)). The parameters governing the quality of the a-Si:H(i) passivation, according to the amphoteric model, are then the total density of recombination centers (N_s), characteristic of the chemical passivation quality, and the charge density at the interface (Q_s), an indicator of the magnitude of the field-effect passivation [44].

By measuring the lifetime in a set of samples with different thicknesses, we can decouple the effects of TR treatment on the surface from the measured effective lifetime. We found that not only the evaluated SRV values after TR in N_2 are surprisingly much higher than those for the wafers held back from any TR treatment, but that the T-dependence of

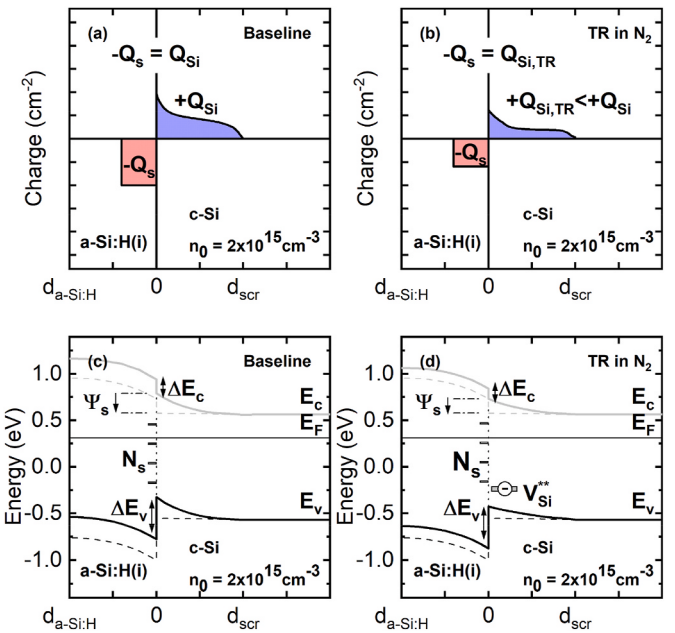


Fig. 7. Charge density diagram for the baseline (a) and for the TR treated sample (b). Band diagram at the passivated c-Si(n) in the dark and under illumination (dashed lines) for the baseline (c) ad for the TR treated sample (d). For the TR in N_2 treated sample, a lower electron diffusion current reduces the charge density Q_s at the a-Si:H(i) in contrast to the baseline case. Less electrons diffuse into the a-Si:H(i) from the c-Si(n) since the underlying vacancies states of the c-Si(n) surface attain electrons due to their proximity to the valence band and the n-type nature of the wafer. (c) A lower electron diffusion current into the a-Si:H(i) decreased the charge density Q_s which reduces the band bending and hence, the field-effect passivation.

the SRV is completely reversed from the expected T-dependence of the a-Si:H(i)-c-Si(n) interface passivation [16,26]. This behavior is better shown in Fig. 8(a) in a SRV as a function of temperature graph, where the open symbols represent the behavior of the SRV for baseline wafers and the solid symbols depict the TR processed ones. This clearly points out that the TR process in N_2 impacts the near surface of the n-type Cz-Si. The recombination at the surface decreases as the temperature of the wafer increases. Note that the observed SRV behavior is repeatable. Multiple measurements of the same samples yielded the same results, suggesting that the effect is not a one-time increase in surface quality by the potential reorganization and diffusion of hydrogen from the a-Si:H(i)

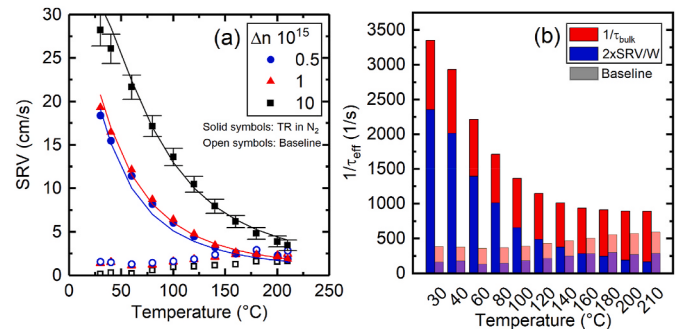


Fig. 8. (a) SRV T-dependence evaluated at three different injection levels along with the fits obtained by applying the recombination model at the interface proposed by Olibet et al. [40] after TR (solid lines). The error bar reported only for the injection level of 10^{16} cm^{-3} specify the uncertainty with the linear regression exemplified in equation (1) (The open symbols reproduce the behavior of the SRV for no TR wafers). (b) Contribution of the surface to the effective lifetime after TR in N_2 . Surface recombination dominates for process-degraded wafers at low temperatures.

[45].

The implication of Fig. 8(a) is visualized in Fig. 8(b) as the breakdown of the τ_{eff} for an injection level of 10^{15} cm^{-3} . At room temperature, approximately 70% of the measured recombination originates at the surface. As the temperature increases, it is reduced to about 20%. The dramatic increase and the T-dependence of the SRV could be linked to recombination mechanisms happening at the a-Si:H(i)/c-Si(n) interface. This is also visualized in Fig. 2(a) where the measured τ_{eff} decreases with the increasing temperature in contrast to Fig. 3(a) where the measured τ_{eff} increases with the increasing temperature. However, it is not immediately clear whether this change in the SRV is predominantly due to a chemical passivation effect or field passivation effect.

To discuss the increase of the recombination rate at the surface after TR in N_2 , we modeled the SRV for different combinations of N_s and Q_s parameters for the a-Si:H(i)/c-Si(n) structure using the recombination model at the interface proposed by Olibet et al. [44]. When modeling the SRV, the following parameters for the interface dangling bond capture cross sections were kept constant and in agreement with the results reported in literature [44,46,47]: $\sigma_p^0/\sigma_n^0 = 20$ and $\sigma_n^+/\sigma_n^0 = \sigma_p^-/\sigma_n^0 = 500$. We also assume $\sigma_p^0 = 10^{-16} \text{ cm}^2$. Our goal is to determine the most likely mechanism, chemical or field-effect passivation, behind the T-dependence of the observed SRV after TR.

Figure 9 illustrates that the SRV experimental data could be satisfactorily reproduced using the Olibet's amphoteric model [44]. On the contour map, we can observe that the parameter Q_s plays a role for values above $\sim 6 \times 10^{10} \text{ cm}^{-2}$. For a Q_s below such value, the SRV is governed by the total density of recombination centers N_s . Considering that the TR in N_2 and the baseline sample received the same surface treatment, and the substrates were passivated using the same a-Si:H(i) deposition conditions, we expect the total density of recombination centers N_s to remain approximately the same for the two experimental conditions. Furthermore, the defect density N_s is not expected to change with increasing temperature. As Seif et al. [26] suggest, the T-dependence SRV of a-Si:H(i) symmetric passivated n-type Si wafers could be tentatively explain by a change in the internal electrical field close to the interface Q_s at high temperature. Bernardini et al. [16] validate this theory by depositing an additional n-type doped layer of a-Si:H on already characterized a-Si:H(i)/c-Si(n)/a-Si:H(i) structures. The SRV T-dependence vanishes since the charge near the surface is set by the fixed charge in the n-doped a-Si:H. Thus, to model the SRV after TR in N_2 , only the charge density at the interface Q_s is adjusted, whereas the total density of recombination centers N_s is kept constant at 10^{10} cm^{-2} to

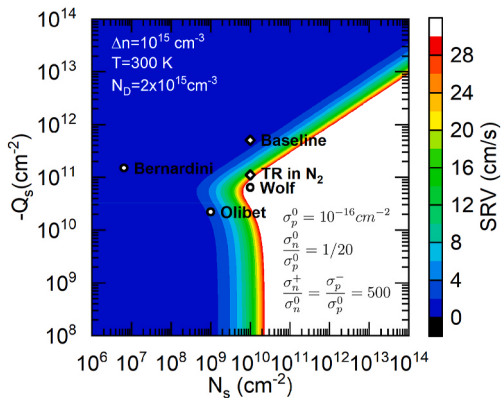


Fig. 9. Modeled SRV for different combinations of N_s and Q_s using the recombination model at the interface proposed by Olibet et al. [40] at room temperature and injection level of 10^{15} cm^{-3} . The diamond symbols depict the parameters that best describe the experimental evaluated SRV at room temperature for an injection level of 10^{15} cm^{-3} in this study (Fig. 8(a)). The round symbol shows the parameter proposed by other authors [40,42,43]. Note that these authors have used different substrate doping and considered different σ_p^0 values.

fit the measured SRV to the Olibet's amphoteric model. Figure 8(a) shows that a good fit of the experimental data temperature-dependence at all injection levels is obtained. From these results the surface charge density Q_s and its T-dependence could be assessed. It has to be noted that the values for N_s and Q_s are in good agreement with previously reported results as shown by the open round symbols in Figure 9 [44,46,47]. It is found that the increase of surface recombination after the TR treatment could be linked to a loss of field-effect passivation, i.e. a decreasing of the surface charge density Q_s . The modeling reveals that the surface charge density at the interface, Q_s , has decreased to $\sim 1 \times 10^{11} \text{ cm}^{-2}$ at 30°C for an injection level of 10^{15} cm^{-3} , about 5 times compared to the sample without TR treatment (see Fig. 9). The analysis of the temperature behavior of the SRV using the amphoteric model [44] also reveals that the surface charge density Q_s T-dependence is governed by Boltzmann distribution with expression $Q_s = -9.9 \times 10^{12} \exp(-0.117/k_B T) \text{ cm}^{-2}$. The previous expression provides a good fit for the injection levels of $5 \times 10^{14} \text{ cm}^{-3}$ and 10^{15} cm^{-3} . The same expression but with a pre-factor of 1.5×10^{13} yields a better fit for the injection level of 10^{16} cm^{-3} , this suggest that the surface charge density Q_s is injection dependent as proposed by Leendertz et al. [48]. The approximation of a fixed charge density for all injection assumes constant quasi-Fermi levels. Leendertz et al. explain that this assumption is not strictly true as there is a gradient in the quasi-Fermi levels under illumination.

As a result of the Boltzmann T-dependence of the surface charge density Q_s , there is an increase in surface potential with rising temperature, resulting in increased electron density and reduced hole density at the surface. Consequently, the surface recombination is weaker by the reduction of one carrier type at high temperatures.

We hypothesize that such behavior of the surface charge density Q_s observed after the TR in N_2 is a consequence of a reduced electron diffusion current into the a-Si:H(i) from the degraded c-Si(n). It is worth mentioning again that the passivation of c-Si(n) with a-Si:H(i) results in the diffusion of electrons (majority carriers) into the a-Si:H(i). In the case of the TR in N_2 treated c-Si(n) wafer, the diffusion of electrons into the a-Si:H(i) decreases as electrons would occupy the bulk states created by the vacancy-associated defects (Fig. 7(d)). In contrast to the untreated wafer, less electrons diffuse into the a-Si:H(i), decreasing the surface charge density Q_s , and consequently, the surface becomes less depleted (Fig. 7(d)) reducing the magnitude of the field-effect passivation explaining the increase in the recombination activity at the surface in the TR in N_2 wafer. As the temperature increases, defect interactions in the bulk of the c-Si(n) play a role in weakening the recombination activity at the interface. We explained in the bulk section how the thermal emission of holes from the defect intensifies as temperature rises, hence there is an increase in the electron diffusion current into the a-Si:H(i) increasing the surface charge density Q_s . Falster [30] reported that the TR gas ambient plays a prominent role in the resulting vacancy concentration profile. Pure nitrogen can contribute to the injection of excess vacancies into the wafer from the surfaces resulting in a U-shaped vacancy profile with an accumulation of vacancies near the surface which supports the hypothesis of near surface vacancy-associated bulk defects playing a role in the reduce diffusion of electrons into the a-Si:H(i) for TR treated wafers.

5. Conclusions

In this work, we have used temperature-injection-dependent lifetime spectroscopy (T-IDLS) to analyze the impact of the application of Tabula Rasa on the minority carrier lifetime of n-type Cz-Si. The effective lifetime of samples with different thicknesses after Tabula Rasa in N_2 , or absence of, were measured to assess the impact of the thermal process on the bulk lifetime and the silicon surfaces expressed by the surface recombination velocity (SRV). We demonstrate that even for carrier lifetime process-degraded wafers, the commonly accepted assumption $\tau_{eff} = \tau_{bulk}$ is no longer valid, and an experimental measure of the SRV is

needed for the analysis of the contribution from τ_{bulk} to τ_{eff} . We use the defect parameter contour mapping (DPCM) methodology to validate that the most likely bulk lifetime limiting defect is a deep double donor vacancy-associated defect with energy 0.13 eV from the valence band edge for TR-treated samples in N₂. We report a capture cross section ratio k~600. To the best knowledge of the authors, this parameter has not been reported before. We show that the TR in N₂ process also significantly (~20 times) increases the surface recombination velocity by a-Si:H(i) passivation layer. The increased surface recombination can be modeled by a decrease in the surface charge density Q_s, and the latter follows a Boltzmann T-dependence. We hypothesize that such behavior results from near surface vacancy-associated bulk defects playing a role in lowering the electron diffusion current into the a-Si:H(i) from the c-Si (n) which reduces the field-effect passivation.

CRediT authorship contribution statement

Jorge Ochoa: Software, Methodology, Formal analysis, Data curation, Conceptualization, Investigation, Visualization. **Vincenzo LaSavia:** Resources, Methodology, Writing – review & editing. **Paul Stradins:** Supervision, Funding acquisition, Writing – review & editing. **Mariana I. Bertoni:** Supervision, Methodology, Formal analysis, Conceptualization, Project administration, Visualization, Writing – review & editing.

Appendix

A Lifetime Measurements

An accurate determination of the recombination lifetime is a fundamental prerequisite for lifetime spectroscopy, this section discusses the techniques used in the present work for measuring the effective carrier lifetime.

Lifetime Tester Calibration

We use a WCT-120TS lifetime tester for Temperature dependence carrier lifetime measurements. The WCT-120TS was calibrated to account for the coil sensitivity error since we measured thin samples. Wafers with different resistivities and stacks of them with different permutations were used to cover a wide range of measured voltages following the methodology given by Ref. [21]. The calibration parameters shown in Fig. 10 were determined by the tester calibration software version 5.0.

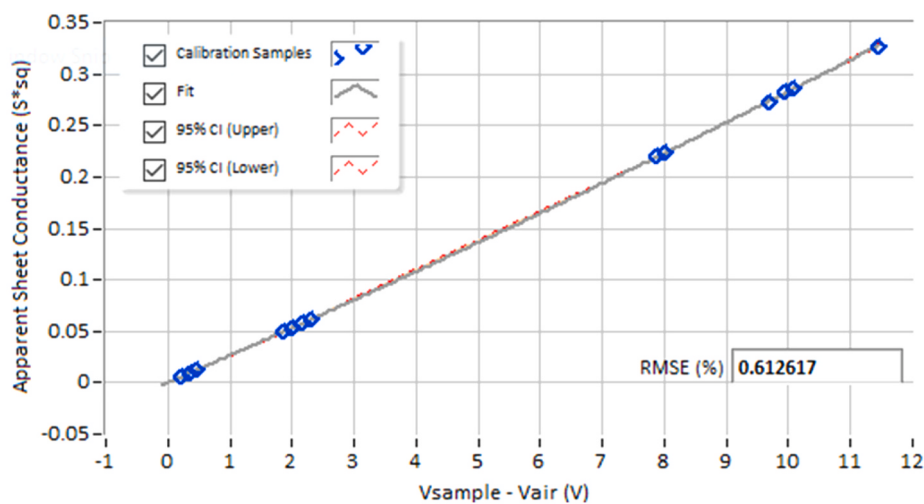


Fig. 10. Calibration data for the Sinton lifetime tester WCT-120TS.

Table 1

WCT-120TS calibration parameters resulting from the measurement of wafers with different resistivities and stacks of them shown in the figure above.

	A ($\text{S}\square/\text{V}^2$)	B ($\text{S}\square/\text{V}$)	OFFSET (V)	λ (MM)
VALUE	0.000223	0.026063	0.006407	3.5162
UNCERTAINTY	3.420738×10^{-5}	0.000268	0.003845	–

Discussion on the range of injection level for SRH analysis

The effective lifetime arises from the superposition of the different recombination processes in the lifetime spectra shown in Fig. 11. It is widely accepted that the bulk lifetime is heavily limited by the Auger recombination at carrier densities $\Delta n > 10^{16} \text{ cm}^{-3}$ [23,24]. Lifetime data points at such excess carrier densities do not contain relevant spectroscopy information for the SRH therefore we limited the analysis to $\Delta n < 10^{16} \text{ cm}^{-3}$.

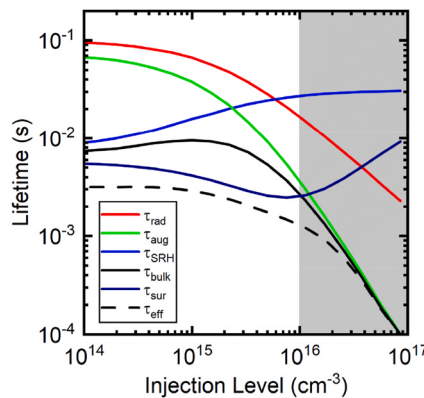


Fig. 11. Modeled recombination components that contribute to the effective lifetime τ_{eff} (black dash line). For excess carrier densities $\Delta n > 10^{16} \text{ cm}^{-3}$ the main limiting factor of the τ_{bulk} (solid black line) is the Auger recombination process (solid green line).

Transient Photoconductance Decay measurements

The measurement of carrier lifetimes is based on the recombination dynamics of excess carriers generated optically. The different techniques may be classified in terms of the time dependence of the illumination and the technique used to measure the excess carrier density. In this work, the effective lifetime was measured by the transient photoconductance decay method. In the transient photoconductance decay method the sample is subject of a short pulse of light that peaks and decay rapidly. The Sinton WCT-120TS measures the decay of the sheet conductance as a function of time which is latter converted by the software to excess carrier density for each moment in time according to $\Delta n = \Delta\sigma/qW(\mu_n + \mu_p)$ and the carrier lifetime at each excess carrier density Δn is determined by taking the derivative of the excess carrier density with respect to time, i.e. the lifetime is determined via $\tau = -\Delta n/(d\Delta n/dt)$ [50–52]..

Since the measurement relies on the derivative $d\Delta n/dt$, it can be affected by signal noise in the low carrier concentration part of the curve. This problem was largely eliminated by averaging with the short flashes required for the transient technique. In the high carrier concentration part of the curve oversaturation of the measurement signal may occur. Then, the maximum minority carrier density of the measurement is given by the lifetime-generation product (τG) [50–52]. It is assumed that lamp light decay is exponential in time with a generation rate $G(t) = 0$ for $t \leq 0$; $G_0 \exp(-t/\tau_{\text{flash}})$ for $t > 0$. As described by Rougieux et al. [49], the transient and generalized lifetime can be considered equal in the case when the carrier profiles remain approximately uniform during the transient decay. This in turn will be true when the minority carrier diffusion length is greater than the sample thickness, and the initial rapid transient modes are excluded from the analysis. These conditions are satisfied for our samples, so it is assumed that at the peak of the transient illumination the lifetimes are equal, $\tau_{\text{transient}} = \tau_{\text{QSS}} = \tau G$. The oversaturation of the reference cell (G) or the sample lifetime (τ) may limit the useful data at high carrier level injection. Efforts in the lifetime measurement setup were taken to avoid saturating the WTC-120TS DAQ ranges, however few points remained out of range. An option is to ignore these data points as they have no meaning, however doing so could raise concerns about the accuracy of the measured lifetime.

The WTC-120TS software V5.10 determines the derivative $d\Delta n/dt$ as default, by using a 2-point slope with Savitzky–Golay method. In general, a 2-point slope method is susceptible to the incorporation of noise due to the fact of averaging in a sub-set of 2 points for the numerical derivative calculation hence the application of the Savitzky–Golay filter to smooth the signal. Sinton Instruments have worked on optimizing a curve smoothing routine and it have been implemented in the standard WCT-120 software, but it has not yet been rolled out to the TS software yet. In an effort to improve the accuracy of the lifetime spectroscopy analysis of this work, Sinton Instruments implemented a preliminary version V5.11.03 giving us access to three methods: 2-point slope, 2-point slope with Savitzky–Golay and 5-point slope.

Figure 12 shows the results of applying the three methodologies to our lifetime data for the thicker sample in the Baseline set. Overall, the 3 methods give similar results, however, discrepancies can be observed at high-level injections. In the case of the 2-point slope with Savitzky–Golay method (the method applied in this manuscript) shown in Fig. 12(a), the filter is applied with the purpose of smoothing the data. It can be seen in Fig. 12 that the lifetime spectra in Fig. 12(b) and (c) exhibits a higher level of noise at low-injection levels compared to (a). The downside of such signal processing is that the lifetime spectra is misreported at $\Delta n > 10^{16} \text{ cm}^{-3}$ as result of the application of the Savitzky–Golay filter in data points saturating the Data Acquisition (DAQ). The Savitzky–Golay filter fits successive sub-sets of adjacent data points including the saturated DAQ data with a polynomial function. Because of the steep slope of the lifetime signal at high carrier densities and the consideration of a saturated data point in the solution of the polynomial fitting, the filter solves a polynomial using the wrong data point which in consequence distorts the signal tendency. Higher lifetimes are likely to be more affected by these artifacts as the excess carrier density signal exhibits a steeper slope at high-level injections. One could also note that the Savitzky–Golay filters are most used to obtain the smoothed derivative value at the central point. Various strategies can be employed

to calculate the points at the start and end of the series however these strategies can lead to the distortion of the signal. The application of the 2-point slope method does not distort lifetime signal tendency at high-level injections, however the spectra display a much noisier signal in the low injection regime, which is less ideal for SRH analysis. Finally, in the case of the 5-point slope the number of sub-sets of adjacent data points considered in the derivative calculation is larger (as the name suggests), therefore DAQ saturated points are considered in a 5-point sub-set of points having an impact in the evaluation of the signal tendency. As a result, the lifetime signal is overestimated as seen in Fig. 12(c). Note that while the noise level is higher for the 2- and 5-point slope methods, the overall shape of the lifetime curves and values are the same for $\Delta n < 10^{16} \text{ cm}^{-3}$ across methods.

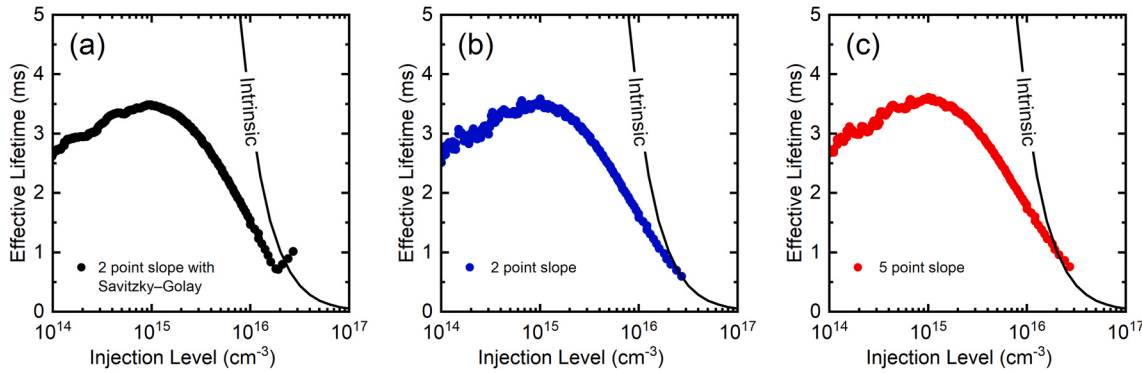


Fig. 12. Reported effective lifetime τ_{eff} at room temperature for the thicker sample ($W = 175 \mu\text{m}$) of the Baseline series of thicknesses. (a) τ_{eff} from 2-point slope with Savitzky-Golay derivative calculation method. (b) τ_{eff} from 2-point slope. (c) τ_{eff} from 5-point slope. The lifetime spectra show that the shape of the lifetime at $\Delta n > 10^{16}$ is affected when a different method to calculate the derivative is selected.

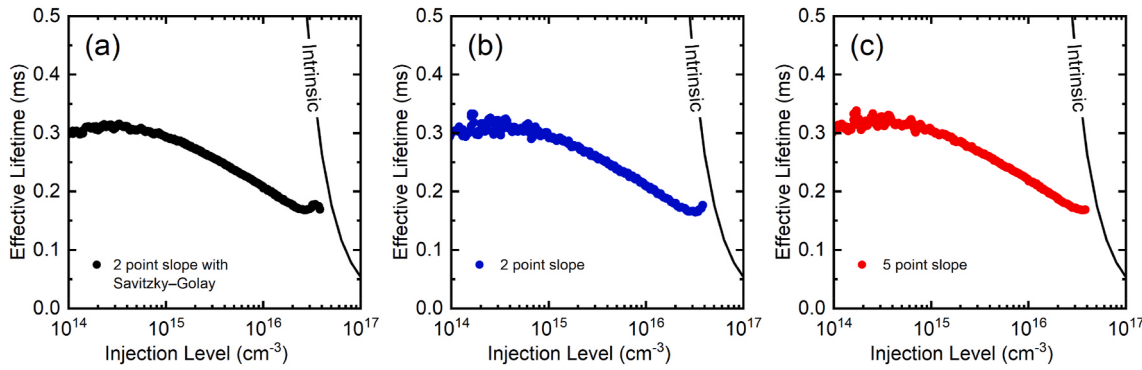


Fig. 13. Reported effective lifetime τ_{eff} at room temperature for the thicker sample ($W = 175 \mu\text{m}$) of the TR treated series of thicknesses. (a) τ_{eff} from 2-point slope with Savitzky-Golay derivative calculation method. (b) τ_{eff} from 2-point slope. (c) τ_{eff} from 5-point slope. The lifetime spectra show that the shape of the lifetime at $\Delta n > 10^{16}$ is affected when a different method to calculate the derivative is selected.

The same analysis was conducted in the lifetime measurement of the thicker sample in the TR treated set. Figure 13 shows the resulting lifetime spectra after using the three different derivative calculation methods. As mentioned above, because the lifetime values are lower than the baseline and the signal exhibits a shallow slope at high-level injections, the signal distortion resulting from the effect of the DAQ saturated data points is much lower.

Finally, for the sake of clarity on the accuracy of the lifetime measurements in this work, Figs. 14 and 15 show the application of the three different derivative calculation methods to the Temperature and injection dependent lifetime data for the thicker wafer in the baseline set and the TR in N_2 respectively. We apply the 2-point slope with Savitzky-Golay in this study to improve the accuracy of the lifetime spectra at low-level injection as this is the spectra that contains the most relevant information for the SRH analysis.

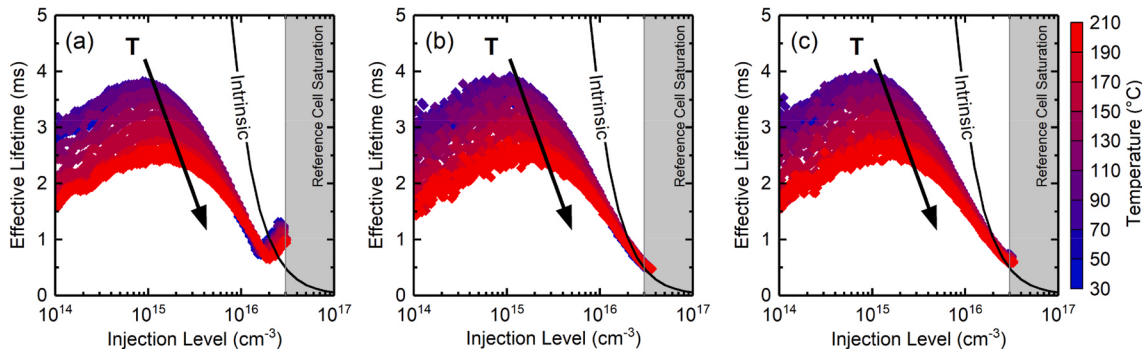


Fig. 14. Reported effective lifetime τ_{eff} for the thickest sample ($W = 175 \mu\text{m}$) in the Baseline set as a function of injection level at temperatures with 10°C step size. (a) τ_{eff} from 2-point slope with Savitzky-Golay derivative calculation method. (b) τ_{eff} from 2-point slope. (c) τ_{eff} from 5-point slope. The spectra show that the shape of the lifetime at $\Delta n > 10^{16}$ is affected when a different method to calculate the derivative is selected. Overall, the three methods give similar result for low injection levels however the noisy is considerably reduce by the application of the Savitzky-Golay filter as shown in (a).

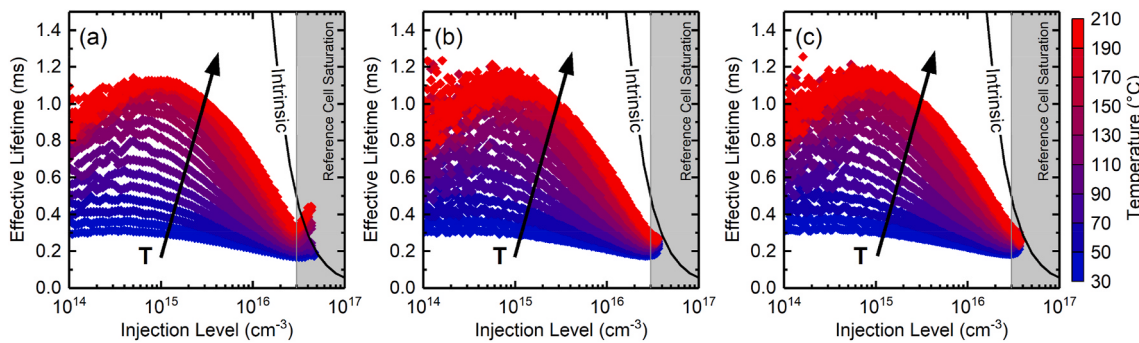


Fig. 15. Reported effective lifetime τ_{eff} for the thickest sample ($W = 175 \mu\text{m}$) in the TR treated set as a function of injection level at temperatures with 10°C step size. (a) τ_{eff} from 2-point slope with Savitzky-Golay derivative calculation method. (b) τ_{eff} from 2-point slope. (c) τ_{eff} from 5-point slope. The spectra show that the shape of the lifetime at $\Delta n > 10^{16}$ is affected when a different method to calculate the derivative is selected. Overall, the three methods give similar result for low injection levels however the noisy is considerably reduce by the application of the Savitzky-Golay filter as shown in (a).

B. Experimental SRV from thickness variation

As given in equation (1), measuring the effective lifetime in a set of samples with different thicknesses allows for the evaluation of the SRV from the slope of plotting recombination rate vs. inverse thickness at every analyzed injection density and at every measured temperature. The goodness of fit was evaluated by the coefficient of the determination R^2 for every injection and every temperature, and such R^2 values are consistently above 90%. Fig. 16 shows the goodness of the linear fit for the set of samples with different thicknesses after TR in N_2 treatment analyzed in this work.

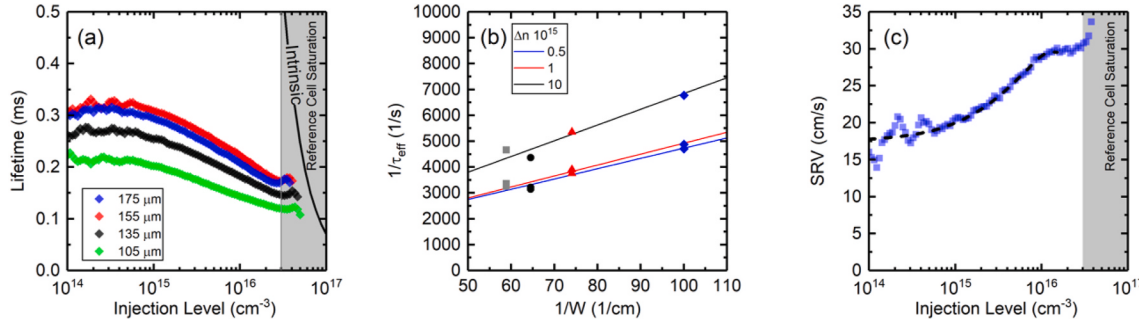


Fig. 16. (a) Measured effective lifetime at 30°C in a set of samples with different thicknesses after TR in N_2 treatment. (b) Recombination rate vs. inverse thickness plot shows the goodness of the fit for three different injection levels at room temperature. (c) SRV vs. Injection level plot shows the experimental evaluated SRV.

At low carrier concentrations weak signals are measured and small signal artifacts have a strong impact hence the noise is more pronounced. The resulting set of SRV curves were smoothed using a LOWESS function as a method to reduce the noise propagated for the extraction of bulk from the thickness variation. The solid line in the SRV vs. Injection level plot from Fig. 16 illustrates the SRV data used to extract the bulk lifetime from the measured effective lifetime.

C. Goodness of the fit to τ_{bulk} for the defect parameters obtained from the DPCM analysis

The goodness of fitting the defect parameters $E_t - E_v = 0.13 \text{ eV}$ and $k = 600$ to the determined bulk lifetime at 30°C is shown in Fig. 17. It must be noted that the DPCM analysis is restricted to the injection level range $5 \times 10^{14} \text{ cm}^{-3}$ to 10^{16} cm^{-3} . We consider these range of injection show the more relevant features of the determined τ_{bulk} . As explained by Bernardini et al. [16], in the DPCM method, the choice of the number of injection levels to be compared and their values can be modified to account for characteristic features in the lifetime curve at a certain injection level which would help obtaining a more univocal fit. We choose injections above $5 \times 10^{14} \text{ cm}^{-3}$ to omit more pronounced noise areas as well as we stay below 10^{16} cm^{-3} because at high level injections Auger recombination is expected to dominate. The effective lifetime at 30°C (Fig. 17 empty dots) is reproduced for comparison. It does not show a clear path above the intrinsic limit. It should be noted that as discussed above, the effective lifetime at room temperature is considerably governed by the surface recombination as well as the limitation of the lifetime measurement for high injection levels. Note that as mentioned above the spectroscopy analysis is conducted in the range $5 \times 10^{14} < \Delta n < 10^{16} \text{ cm}^{-3}$.

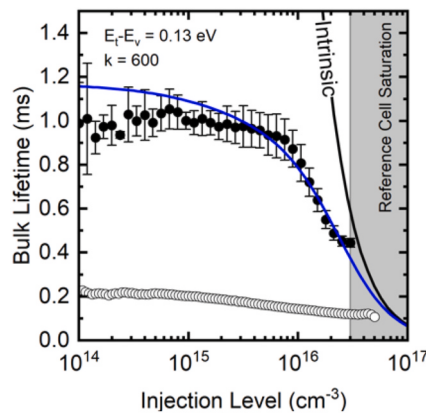


Fig. 17. Bulk lifetime as a function of injection level at 30 °C. The blue solid line illustrates the goodness of fitting the defect parameters $E_t - E_v = 0.13$ eV and $k = 600$ to the determined bulk lifetime at 30 °C. The black dots with error bar report the standard deviation of the determined τ_{bulk} from the different thicknesses. The effective lifetime at 30 °C (empty dots) is reproduced for comparison.

References

- [1] Jan Schmidt, Temperature- and injection-dependent lifetime spectroscopy for the characterization of defect centers in semiconductors, *Appl. Phys. Lett.* 82 (13) (2003) 2178–2180.
- [2] Daniel Macdonald, L.J. Geerligs, Recombination activity of interstitial iron and other transition metal point defects in p- and n-type crystalline silicon, *Appl. Phys. Lett.* 85 (18) (2004) 4061–4063.
- [3] Jeanette Lindroos, Hele Savin, Review of light-induced degradation in crystalline silicon solar cells, *Sol. Energy Mater. Sol. Cell.* 147 (2016) 115–126.
- [4] Richard M. Swanson, Approaching the 29% limit efficiency of silicon solar cells, in: Conference Record of the Thirty-First IEEE Photovoltaic Specialists Conference, 2005, pp. 889–894, 2005.
- [5] David D. Smith, Peter Cousins, Staffan Westerberg, Russelle De Jesus-Tabajonda, Gerly Aniero, Yu-Chen Shen, Toward the practical limits of silicon solar cells, *IEEE J. Photovoltaics* 4 (6) (2014) 1465–1469.
- [6] Peter J. Cousins, David D. Smith, Hsin-Chiao Luan, Jane Manning, Tim D. Dennis, Ann Waldhauer, Karen E. Wilson, Gabriel Harley, and William P. Mulligan. Generation 3: improved performance at lower cost, in: 2010 35th IEEE Photovoltaic Specialists Conference, 2010, 000275–000278.
- [7] S.W. Glunz, J. Benick, D. Biro, M. Bivour, M. Hermle, D. Pysch, M. Rauer, C. Reichel, A. Richter, M. Rüdiger, C. Schmiga, D. Suwito, A. Wolf, R. Preu, n-type silicon - enabling efficiencies > 20% in industrial production, in: 2010 35th IEEE Photovoltaic Specialists Conference, 2010, 000050–000056.
- [8] G. Coletti, P. Manshanden, S. Bernardini, P.C.P. Bronsveld, A. Gutjahr, Z. Hu, G. Li, Removing the effect of striations in n-type silicon solar cells, *Sol. Energy Mater. Sol. Cell.* 130 (2014) 647–651.
- [9] J.D. Murphy, K. Bothe, V.V. Voronkov, R.J. Falster, On the mechanism of recombination at oxide precipitates in silicon, *Appl. Phys. Lett.* 102 (4) (2013), 042105.
- [10] Dominic Walter, Bianca Lim, R. Falster, Jeff Binns, Jan Schmidt, Understanding lifetime degradation in czochralski-grown n-type silicon after high-temperature processing, volume 2DP 1 (1) (2013) 699–702, 09.
- [11] Vincenzo LaSalvia, Amanda Youssef, Mallory A. Jensen, Erin E. Looney, William Nemeth, Matthew Page, Wooseok Nam, Tonio Buonassisi, Stradins Paul, Tabula Rasa for n-Cz silicon-based photovoltaics, *Prog. Photovoltaics Res. Appl.* 27 (2) (2019) 136–143.
- [12] Rabia Basnet, Fiacre E. Rougier, Chang Sun, Sieu P. Phang, Chris Samundsett, Roland Einhaus, Julien Degoulange, and Daniel MacDonald. Methods to improve bulk lifetime in n-type czochralski-grown upgraded metallurgical-grade silicon wafers, *IEEE J. Photovoltaics* 8 (4) (2018) 990–996.
- [13] J. Falster Robert, M. Cornara, D. Gambaro, M. Olmo, M. Pagani, Effect of high temperature pre-anneal on oxygen precipitates nucleation kinetics in Si, *Solid State Phenom.* 57–58 (1997) 123–128.
- [14] D.C. Walter, B. Lim, K. Bothe, V.V. Voronkov, R. Falster, J. Schmidt, Effect of rapid thermal annealing on recombination centres in boron-doped Czochralski-grown silicon, *Appl. Phys. Lett.* 104 (4) (2014), 042111.
- [15] Abigail R. Meyer, Vincenzo LaSalvia, William Nemeth, Wanxing Xu, Matthew Page, David L. Young, Sumit Agarwal, and Paul Stradins. Influence of Tabula Rasa on process- and light-induced degradation of solar cells fabricated from czochralski silicon, *IEEE J. Photovoltaics* 10 (6) (2020) 1557–1565.
- [16] Simone Bernardini, Tine U. Nærland, Adrienne L. Blum, Gianluca Coletti, Mariana I. Bertoni, Unraveling bulk defects in high-quality c-Si material via TIDLS, *Prog. Photovoltaics Res. Appl.* 25 (3) (2017) 209–217.
- [17] Simone Bernardini, Tine U. Nærland, Gianluca Coletti, Mariana I. Bertoni, Defect parameters contour mapping: a powerful tool for lifetime spectroscopy data analysis, *Phys. Status Solidi* 255 (8) (2018), 1800082.
- [18] S. Rein, T. Rehrl, W. Warta, S.W. Glunz, Lifetime spectroscopy for defect characterization: systematic analysis of the possibilities and restrictions, *J. Appl. Phys.* 91 (4) (2002) 2059–2070.
- [19] Stefan Rein, Lifetime Spectroscopy, A Method of Defect Characterization in Silicon for Photovoltaic Applications, Springer Series in Material Science, 2005.
- [20] Yan Zhu, Ziv Hameiri, Review of injection dependent charge carrier lifetime spectroscopy, *Progress Energy* 3 (1) (2021), 012001.
- [21] Lachlan E. Black, Daniel H. Macdonald, Accounting for the dependence of coil sensitivity on sample thickness and lift-off in inductively coupled photoconductance measurements, *IEEE J. Photovoltaics* 9 (6) (2019) 1563–1574.
- [22] Jan Schmidt, Armin G. Aberle, Accurate method for the determination of bulk minority-carrier lifetimes of mono- and multicrystalline silicon wafers, *J. Appl. Phys.* 81 (9) (1997) 6186–6199.
- [23] A. Richter, F. Werner, A. Cuevas, J. Schmidt, S.W. Glunz, Improved parameterization of auger recombination in silicon, *Energy Proc.* 27 (2012) 88–94.
- [24] T. Niewelt, B. Steinhauser, A. Richter, B. Veith-Wolf, A. Fell, B. Hammann, N. E. Grant, L. Black, J. Tan, A. Youssef, J.D. Murphy, J. Schmidt, M.C. Schubert, S. W. Glunz, Reassessment of the intrinsic bulk recombination in crystalline silicon, *Sol. Energy Mater. Sol. Cell.* 235 (2022), 111467.
- [25] Hieu T. Nguyen, Simeon C. Baker-Finch, Daniel Macdonald, Temperature dependence of the radiative recombination coefficient in crystalline silicon from spectral photoluminescence, *Appl. Phys. Lett.* 104 (11) (2014), 112105.
- [26] Johannes P. Seif, Gopal Krishnamani, Benedicte Demaurex, Christophe Ballif, Stefaan De Wolf, Amorphous/Crystalline silicon interface passivation: ambient-temperature dependence and implications for solar cell performance, *IEEE J. Photovoltaics* 5 (3) (2015) 718–724.
- [27] W. Shockley, W.T. Read, Statistics of the recombinations of holes and electrons, *Phys. Rev.* 87 (5) (1952) 835–842.
- [28] M. Jacob, P. Pichler, Heiner Ryssel, Robert J. Falster, M. Cornara, D. Gambaro, M. Olmo, M. Pagani, Observation of vacancy enhancement during rapid thermal annealing in nitrogen, *Solid State Phenom.* 57–58 (1997) 349–354.
- [29] R. Falster, D. Gambaro, M. Olmo, M. Cornara, H. Korb, The engineering of silicon wafer material properties through vacancy concentration profile control and the achievement of ideal oxygen precipitation behavior, *MRS Proceedings* 510 (1) (1998) 27.
- [30] Robert J. Falster, Vladimir V. Voronkov, Rapid thermal processing and the control of oxygen precipitation behaviour in silicon wafers, *Mater. Sci. Forum* 573–574 (2008) 45–60.
- [31] V.V. Voronkov, R. Falster, P. Pichler, Relaxation of vacancy depth profiles in silicon wafers: a low apparent diffusivity of vacancy species, *Appl. Phys. Lett.* 104 (3) (2014), 032106.
- [32] Vladimir Voronkov, Robert Falster, Multiple structural forms of a vacancy in silicon as evidenced by vacancy profiles produced by rapid thermal annealing, *Phys. Status Solidi* 251 (11) (2014) 2179–2184.
- [33] Peter Pichler, Intrinsic point defects, impurities, and their diffusion in silicon, *Comput. Microelectronic.* (2004) 77–227.
- [34] J.L. Newton, A.P. Chatterjee, R.D. Harris, G.D. Watkins, Negative-U properties of the lattice vacancy in silicon, *Phys. B+C* 116 (1–3) (1983) 219–223.
- [35] G.D. Watkins, J.R. Troxell, Negative-U properties for point defects in silicon, *Phys. Rev. Lett.* 44 (9) (1980) 593–596.
- [36] J.R. Troxell, G.D. Watkins, A.P. Chatterjee, Vacancies and Interstitials in Silicon, Institute of Physics, United Kingdom, 1978, 1.
- [37] F. Stöckmann, On the classification of traps and recombination centres, *Phys. Status Solidi* 20 (1) (1973) 217–220.
- [38] Tine U. Narland, Simone Bernardini, Marie Syre Wiig, Mariana I. Bertoni, Is it possible to unambiguously assess the presence of two defects by temperature- and injection-dependent lifetime spectroscopy? *IEEE J. Photovoltaics* 8 (2) (2018) 465–472.

- [39] Adrienne L. Blum, James S. Swirhun, Ronald A. Sinton, Fei Yan, Stanislau Herasimenka, Thomas Roth, Kevin Lauer, Haunschild Jonas, Bianca Lim, Karsten Bothe, Ziv Hameiri, Bjoern Seipel, Rentian Xiong, Marwan Dhamrin, John D. Murphy, Interlaboratory study of eddy-current measurement of excess-carrier recombination lifetime, *IEEE J. Photovoltaics* 4 (1) (2013) 525–531.
- [40] R. Schlaf, R. Hinogami, M. Fujitani, S. Yae, Y. Nakato, Fermi level pinning on HF etched silicon surfaces investigated by photoelectron spectroscopy, *J. Vac. Sci. Technol.: Vacuum Surf. Film.* 17 (1) (1999) 164–169.
- [41] A.G. Aberle, Crystalline Silicon Solar Cells: Advanced Surface Passivation and Analysis, University of New South Wales, 2004.
- [42] Stefaan De Wolf, Michio Kondo, Abruptness of a-Si:H/c-Si interface revealed by carrier lifetime measurements, *Appl. Phys. Lett.* 90 (4) (2007), 042111.
- [43] Jan-Willem A. Schüttauf, Karine H.M. van der Werf, Inge M. Kielen, Wilfried G.J. H.M. van Sark, Jatindra K. Rath, Ruud E.I. Schropp, High quality crystalline silicon surface passivation by combined intrinsic and n-type hydrogenated amorphous silicon, *Appl. Phys. Lett.* 99 (20) (2011), 203503.
- [44] Sara Olibet, Evelyne Vallat-Sauvain, Luc Fesquet, Christian Monachon, Aëcha Hessler-Wyser, Jérôme Damon-Lacoste, Stefaan De Wolf, Christophe Ballif, Properties of interfaces in amorphous/crystalline silicon heterojunctions, *Phys. Status Solidi* 207 (3) (2010) 651–656.
- [45] Jonathon Mitchell, Daniel Macdonald, Andres Cuevas, Thermal activation energy for the passivation of the n-type crystalline silicon surface by hydrogenated amorphous silicon, *Appl. Phys. Lett.* 94 (16) (2009), 162102.
- [46] Stefaan De Wolf, Bénédicte Demaurex, Descoeuilles Antoine, Christophe Ballif, Very fast light-induced degradation of a-Si:H/c-Si(100) interfaces, *Phys. Rev. B* 83 (23) (2011), 233301.
- [47] Simone Bernardini, I. Mariana, Bertoni, Insights into the degradation of amorphous silicon passivation layer for heterojunction solar cells, *Phys. Status Solidi* 216 (4) (2019), 1800705.
- [48] C. Leendertz, R. Stangl, T.F. Schulze, M. Schmidt, L. Korte, A recombination model for a-Si:H/c-Si heterostructures, *Phys. Status Solidi* 7 (3–4) (2010) 1005–1010.
- [49] F.E. Rougieux, P. Zheng, M. Thiboust, J. Tan, N.E. Grant, D.H. Macdonald, A. Cuevas, A contactless method for determining the carrier mobility sum in silicon wafers, *IEEE J. Photovoltaics* 2 (1) (2012) 41–46.
- [50] R.A. Sinton, A. Cuevas, M. Stuckings, Quasi-steady-state photoconductance, a new method for solar cell material and device characterization, in: Conference Record of the Twenty Fifth IEEE Photovoltaic Specialists Conference, 1996, pp. 457–460, <https://doi.org/10.1109/pvsc.1996.564042>, 1996.
- [51] R.A. Sinton, T. Trupke, Limitations on dynamic excess carrier lifetime calibration methods, *Prog. Photovoltaics Res. Appl.* 20 (2) (2012) 246–249, <https://doi.org/10.1002/pip.1119>.
- [52] R.A. Sinton, Test methods for contactless carrier recombination lifetime in silicon wafers, blocks, and ingots, SEMI Standard Meet Hamburg, (2009).